The Astrophysical Journal, 642:1193–1204, 2006 May 10

MODELS OF THE LARGE-SCALE CORONA. II. MAGNETIC CONNECTIVITY AND OPEN FLUX VARIATION

D. H. Mackay
School of Mathematics and Statistics, University of St. Andrews, St. Andrews, Fife, Scotland KY16 9SS UK; duncan@mcs.st-and.ac.uk

and

A. A. van Ballegooijen
Harvard-Smithsonian Center for Astrophysics, 60 Garden Street, Cambridge, MA 02138; vanballe@cfa.harvard.edu
Received 2005 October 21; accepted 2005 December 20

ABSTRACT

In this paper the changing connectivity of the coronal magnetic field during the formation and ejection of magnetic flux ropes is considered. Using recent simulations of the coronal field, it is shown that reconnection may occur both above and below the flux ropes. Those occurring above slowly strip away coronal arcades overlying the flux ropes and allow the flux ropes to be ejected. In contrast, those below help to push the flux ropes out. It is found that the reconnection occurring below each flux rope may result in significant skew being maintained within the coronal field above the PIL after the flux rope is ejected. In addition, after the eruption, as the coronal field closes down, the large-scale transport of open flux across the bipoles takes place through the process of "interchange reconnection." As a result, new photospheric domains of open flux are created within the centers of the bipoles, where field lines were previously closed. The net open flux in the simulation may be split into two distinct contributions. The first contribution is due to the nonpotential equilibrium coronal fields of the bipoles. The second contribution is a temporary enhancement to this during the ejection of the flux ropes, where previously closed field lines become open. It is shown that the nonpotential equilibrium contribution to the open flux is significantly higher than that due to a potential field deduced from the same photospheric boundary conditions. These results suggest that the nonpotential nature of coronal magnetic fields may affect the variation of the Sun's open flux during periods of high solar activity and should be considered in future simulations.

Subject headings: Sun: corona — Sun: magnetic fields

1. INTRODUCTION

In the recent paper of Mackay & van Ballegooijen (2006, hereafter Paper I) the response of the large-scale coronal magnetic field to the transport of magnetic flux in the photosphere is investigated using numerical simulations. In particular, the formation and evolution of coronal flux ropes is studied as two bipolar magnetic regions interact with one another. The interaction of the initially sheared but unconnected bipoles is similar to the head-to-tail linkage model of Martens & Zwaan (2001; also see Mackay & van Ballegooijen 2001; Litvinenko & Wheatland 2005; Welsch et al. 2005); the initial shear of a bipole represents the twist of the magnetic field before it emerges into the solar atmosphere. In these simulations a coronal flux rope is defined to be a highly sheared and/or twisted magnetic field located above a polarity inversion line (PIL) of the photospheric magnetic field (Russell et al. 1990; Amari et al. 1999; Low 2001). Understanding the origin and evolution of such flux ropes is of integral importance in understanding the nature of many solar phenomena, including solar filaments (Priest 1989; Martin 1998), solar flares (Priest 1982; Somov 1992), coronal mass ejections (Hundhausen 1993; Low 2001), and sigmoids (Rust & Kumar 1995; Canfield et al. 1999; Pevtsov 2002).

To simulate the evolution of the coronal field over a period of weeks to months, a combination of magnetic flux transport (van Ballegooijen et al. 1998) and magnetofrictional relaxation (Yang et al. 1986; van Ballegooijen et al. 2000) techniques are employed. In this approach initially prescribed surface and coronal fields are sheared by dynamic surface motions. In Paper I these motions include differential rotation, meridional flow, and surface diffusion. These surface motions result in shearing of the coronal field and the formation of coronal flux ropes. The coronal plasma velocity is assumed to be proportional to the Lorentz force, which causes the coronal field to evolve through a series of nonlinear force-free field (NLFFF) states (van Ballegooijen et al. 2000; Mackay et al. 2000; Mackay & van Ballegooijen 2001, 2005; Mackay & Gaizauskas 2003). By constructing NLFFFs through dynamic boundary conditions, the evolution of the large-scale coronal field can be followed for many months. Both highly sheared regions, such as flux ropes, and weakly sheared regions, such as overlying coronal arcades or open flux (Lockwood et al. 1999; Lockwood 2003), can be investigated. This process of simultaneous shearing and relaxing of the coronal field is in contrast to the more commonly used extrapolation techniques with fixed boundary conditions, for example, the construction of linear force-free fields (e.g., Nakagawa & Raadu 1972; Aulanier & Démoulin 1998; Mackay et al. 1999) and the construction of NLFFFs based on vector field data (Mikic & McClymont 1994; McClymont et al. 1997; Régnier et al. 2002; Bleybel et al. 2002).

A key element in the formation of coronal flux ropes is the reconnection of magnetic fields in the photosphere associated with photospheric flux cancellation at polarity inversion lines. Through this cancellation and reconnection, flux ropes may form gradually over periods of days to weeks, both above the external PIL between the two bipoles (representing type B filaments; see Mackay & van Ballegooijen 2005) or above the internal PIL of each bipole in a sigmoid shape. In Paper I it is shown that once a flux rope forms, the coronal field may diverge from equilibrium with the ejection of the flux rope (see also Isenberg et al. 1993; Lin & Forbes 2000; Amari et al. 2003; Török & Kliem 2005). However, after the flux rope is ejected, the coronal field once again relaxes down to an equilibrium (see Paper I, Fig. 5). This ability to follow

the evolution of coronal fields through ejections is essential for future planned full-Sun simulations in which multiple bipoles are evolved for many months or years. The present simulations of two bipoles consider the basic interactions expected to occur for many bipoles in future simulations.

In this paper, the simulations of Paper I are analyzed to determine the connectivity of the coronal field and the reconnections that occur during different phases of the simulation, including the ejection of the flux ropes. Coronal reconnection is found to occur both above and below the flux ropes. Those occurring above open up the overlying field, while those occurring below maintain a significant shear to the field overlying the PIL once the flux ropes are expelled. The coronal reconnection is found to produce the large-scale transport of open flux across the bipoles through the process of "interchange reconnection" (Crooker et al. 2002). It is shown that after all of the flux ropes have formed and been ejected, the coronal field closes down in a connectivity similar to that of the initial connectivity, and a new coronal flux rope begins to form.

The paper is structured as follows. In § 2 a brief description of the model is given; for a more detailed description, along with the justification for using the magnetofrictional approach and choice of model parameters, see Paper I. In § 3 the coronal reconnection that occurs during the ejection of the flux ropes is discussed, and different phases in the evolution of the coronal field are considered. In § 4 the variation of the open flux and its large-scale transport through "interchange reconnection" are discussed. Finally, in § 5 the conclusions of the paper are given.

2. THE MODEL AND SETUP

To consider the formation of coronal flux ropes and the evolution of the large-scale corona, we use a magnetic flux transport and magnetofrictional model. The magnetic field $\boldsymbol{B}(\boldsymbol{r}, t)$ is described in terms of the vector potential ($\boldsymbol{B} = \nabla \times \boldsymbol{A}$), and a spherical coordinate system (r, θ, ϕ) is used. A finite region in the corona is considered, and the field is assumed to be periodic at the longitudinal boundaries of the computational domain. The initial state consists of two magnetic bipoles separated from each other in longitude and initially without any magnetic connections between the bipoles. Each bipole has a small amount of shear representing the twist in the magnetic field prior to its emergence into the solar atmosphere. All of the magnetic helicity needed for the formation of coronal flux ropes is already present in this initial state; there is no flux emergence during the simulation.

The vector potential $\boldsymbol{A}(\boldsymbol{r}, t)$ is evolved according to the magnetic induction equation. The induction equation at $r = R_\odot$ describes the transport of magnetic flux in the photosphere. We include surface transport due to large-scale flows (differential rotation and meridional flows) and smaller scale random flows associated with the supergranulation. The effect of the supergranules is described as a surface diffusion process (Leighton 1964). This diffusion leads to the cancellation and reconnection of opposite-polarity magnetic fields when they encounter one another at PILs. The flux transport equations for the time derivatives of A_θ and A_ϕ at $r = R_\odot$ are given in Paper I. These equations purposely include only the horizontal diffusion of the radial field, not the radial diffusion of the horizontal field. This approach represents what we believe is a real physical effect on the Sun, namely, that the photosphere presents a barrier for the submergence of axial fields at the PIL (van Ballegooijen & Martens 1989).

In the coronal region the magnetic field evolves according to the nonideal induction equation,

$$\frac{\partial \boldsymbol{A}}{\partial t} = \boldsymbol{v} \times \boldsymbol{B} - \eta_c \boldsymbol{j}, \tag{1}$$

where $\boldsymbol{v}(\boldsymbol{r}, t)$ is the plasma velocity, $\boldsymbol{j}(\boldsymbol{r}, t)$ is the current density ($\boldsymbol{j} = \nabla \times \boldsymbol{B}$), and η_c is the coronal diffusivity. We assume that the coronal plasma velocity is given by

$$\boldsymbol{v} = \frac{1}{\nu}\frac{\boldsymbol{j} \times \boldsymbol{B}}{B^2} + v_o e^{-(2.5\,R_\odot - r)/r_w}\hat{\boldsymbol{r}}, \tag{2}$$

where the first term on the right-hand side approximates the effect of the Lorentz force on the coronal plasma (magnetofrictional method; see Yang et al. 1986; van Ballegooijen et al. 2000). By taking the friction coefficient ν to be very small compared to timescales of the photospheric motions, the coronal field is forced to evolve through a series of force-free equilibrium states. The second term in equation (2) is a radial outflow velocity imposed to ensure that the magnetic field remains radial at the source surface ($r = 2.5\ R_\odot$). In a crude manner this outflow velocity simulates the effect that the solar wind would have on opening closed coronal field lines; v_o is the peak velocity, and r_w is the width over which the velocity drops off at the outer boundary. Note that once the field lines become radial, the second term no longer affects the magnetic field. The coronal diffusion is taken to be of the form

$$\eta_c = \eta_o\left(1 + c\frac{|\boldsymbol{j}|}{B}\right), \tag{3}$$

which includes both a background term (first term) and an enhanced term (second term), which only acts in regions of strong current density. The second term mainly acts when twisted flux rope structures are produced and limits the amount of twist within them by decreasing the amount of poloidal flux. Coronal diffusion is included, as in the previous simulations, which assumed ideal magnetohydrodynamics (MHD; Mackay & van Ballegooijen 2001) in the corona for periods of weeks to months produced highly twisted flux rope structures, which are found not to be realistic. In addition to the explicitly prescribed diffusion, numerical diffusion is also present; however, this is significantly less than that prescribed above, so it should not affect the results of the simulation. Details of the numerical grid used, along with boundary conditions, can be found in Paper I. For the simulations we consider a region in the northern hemisphere in the range $1\ R_\odot < r < 2.5\ R_\odot$, $30^\circ < \theta < 100^\circ$ and $0^\circ < \phi < 90^\circ$, with a resolution of $\delta\phi = 0.^\circ5$. The following values of the outflow velocity and diffusion parameters are used: $v_o = 100$ km s^{-1}, $r_w = 0.2\ R_\odot$, $\eta_o = 0.1D$, $c = 0.2\ R_\odot$, and $\nu = 5\delta t/h_\phi^2$, where D is the photospheric diffusion constant. The above values are determined from running a number of test cases (see Paper I).

To produce the initial configuration in Paper I, two bipoles are inserted into an initially empty computational box over a finite region, both in the photosphere and in the corona. Each bipole has a center point with longitude ϕ_0 and latitude λ_0. The initial description of a bipole in terms of the coordinates $[x(\phi), y(\theta), z(r)]$ (see Paper I) relative to the center point is

$$B_x = B_0 e^{0.5}\left(\frac{z}{\rho_0}e^{-\xi} + 4\beta\frac{xy}{\rho_0^2}e^{-2\xi}\right),$$

$$B_y = 2\beta B_0 e^{0.5}\left(1 - \frac{x^2 + z^2}{\rho_0^2}\right)e^{-2\xi},$$

$$B_z = B_0 e^{0.5}\left(-\frac{x}{\rho_0}e^{-\xi} + 4\beta\frac{yz}{\rho_0^2}e^{-2\xi}\right),$$

where $\xi \equiv [(x^2 + z^2)/2 + y^2]/\rho_0^2$, ρ_0 is the half-separation between the peaks of the photospheric flux pattern (corresponding to a heliocentric angle of 5°), B_0 is the peak flux density ($B_0 = -200$ G),

and β is a dimensionless parameter describing the twist of the magnetic field. Positive values of β add a positive twist or helicity to the bipoles, while negative values add a negative twist or helicity. This field description of the bipoles may also be rotated so that the bipoles are given a tilt (γ) consistent with Joy's law.

One bipole is placed at $\phi_0 = 42^\circ$, $\lambda_0 = 17^\circ$ with $\gamma = 10^\circ$, $\beta = -0.3$ and the other at $\phi_0 = 65^\circ$, $\lambda_0 = 17^\circ$ with $\gamma = 10^\circ$, $\beta = -0.2$. Both bipoles are twisted by a different amount so that the flux ropes form and are ejected at different times, making it easier to follow the evolution of the coronal field. Initially, the two bipoles are in a state of extreme nonequilibrium, where in each bipole all of the flux from one polarity connects to the other polarity and there are no cross-connections between the bipoles. To attain equilibrium, the bipoles expand to fill the entire computational volume and cross-connections are made. This process and the subsequent evolution of the surface and coronal fields as they evolve under flux transport effects for a period of 60 days is described in § 2.

3. LARGE-SCALE CORONAL EVOLUTION AND PHOTOSPHERIC CONNECTIVITY DOMAINS

The evolution of the large-scale coronal field and photospheric connectivity domains is now considered as the flux ropes are formed and ejected. Within the simulations reconnection of field lines may occur both in the photosphere and in the corona. In Paper I it is shown that photospheric reconnection is the key to the formation of the flux ropes. Such reconnection can occur as flux converges and cancels at PILs. Along with this, coronal reconnection may also occur in the simulation where there is no cancellation of flux, but rather a changing connectivity of the field lines within each of the bipoles. Such changing connectivity of the field is required so that the overlying coronal arcades above the flux ropes may open up and the flux ropes be expelled.

We now consider the connectivity of the field lines between the four polarities that make up the two bipoles. In the photosphere, four types of connectivity domain can be defined:

1. Bipolar connectivity (b): locations in the photosphere where field lines connect between the two polarities that make up an original bipole.
2. Cross-bipolar connectivity (cb): locations in the photosphere where field lines make cross-connections between the two bipoles and these connections stay within the computational domain.
3. Open connectivity (o): locations in the photosphere where field lines extend up to the source surface at 2.5 $R_\odot$.
4. Periodic connectivity (p): locations in the photosphere where field lines pass through the periodic ϕ-boundaries.

The simulations presented here have a limited longitude range, so the periodic connectivity is deemed to be not real, but an artifact of the boundary conditions (in future full-Sun simulations the periodic connectivity type will be omitted). In calculating the amount of flux within each connectivity domain all grid points on the photosphere with radial fields B_r in excess of ± 0.5 G are considered. In the following one has to keep in mind that diffusion is present both in the photosphere and in the corona, so flux may diffuse out of the ± 0.5 G contours and therefore not be considered from one time step to the next. However, this has only a minor effect on the results of the simulations and the variation of the amount of flux within each domain.

For the 60 day evolution period considered, it is found that surface reconnection involving flux cancellation preserves each of the photospheric connectivity domains. This is because such reconnection occurs across either the internal PIL of each bipole or the external PIL between the two bipoles, involving either two bipolar or two cross-bipolar field lines, respectively, reconnecting to produce another of the same type. Even though such reconnection does preserve the connectivity domains, it decreases the amount of flux within each of the domains. In contrast, when coronal reconnection occurs between field lines from different photospheric connectivity domains, the domains are no longer preserved. The results of the simulation are now discussed in detail, and the connectivity changes during four distinct phases in the evolution of the coronal field (setup, shearing, ejection, and close-down phases) are considered.

3.1. *Setup Phase*

The setup phase occurs between days 0 and 3 in the simulation, when the bipoles are initially inserted into the computational box in nonequilibrium. During this phase, the initial connections are made between the bipoles, and the field lines reduce to equilibrium. The variation of the photospheric connectivity domains defined above over this period can be seen in Figures 1*a*–1*c* for days 0–2; blue represents bipolar connectivity (b), green represents cross-bipolar connectivity (cb), red represents open flux (o), and yellow represents periodic connectivity (p). In addition, the graph in Figure 2*a* shows the variation of the flux lying within each of the connectivity domains as a function of the day of simulation. Each of the lines gives the net unsigned flux summed over each of the bipoles, where bipolar connectivity is given by the dotted line, cross-bipolar flux is given by the dash-dotted line, open flux is given by the dashed line, and periodic flux is given by the triple-dot–dashed line). In addition, the variation of the total flux within the bipoles is plotted as the solid line. The total flux steadily decreases through the simulation, as flux is canceled at PILs due to surface diffusion.

On day 0 from Figures 1*a* and 2*a* it is clear that when the bipoles are inserted, the photospheric flux is essentially all of bipolar connectivity (*blue or dotted line*), and there is very limited cross-connection between the bipoles (*minor areas of green*). However, by day 1 (Fig. 1*b*) the connectivity domains of the bipoles have changed significantly, with cross-bipolar connections present within each of the polarities of the bipoles. These new connectivity domains arise from the bipoles expanding and interacting with one another. At the point where they interact a quasi separator forms (Priest & Démoulin 1995), and oppositely oriented bipolar field lines reconnect with each other to produce cross-bipolar field lines (b + b $\rightarrow$ cb + cb). One cross-bipolar field line lies above the quasi separator, the other below it. This process is outlined in Figure 3*a*, which shows an X-type structure in the corona above the midpoint between the two bipoles, representing the reconnection site and quasi separator. In Figure 2*a* the conversion of bipolar flux to cross-bipolar flux can be seen where the bipolar flux decays faster than the total flux and the cross-bipolar flux increases. Although there appears to be a significant area of cross-bipolar connectivity in Figure 1*b*, this connectivity type only occurs in weak field locations, so the total cross-bipolar flux is small.

Between days 1 and 2 (Figs. 1*b* and 1*c*) there are again significant connectivity changes, and on day 2 both open (*red*) and periodic fluxes (*yellow*) are present. These new connectivity domains lie at the outer edges of the leading and trailing polarities of the two bipoles. The open field lines form as cross-bipolar field lines located above the quasi separator expand and are pulled open by the radial outflow velocity (cb $\rightarrow$ 0). As more and more cross-bipolar field lines are pulled open, the previously open field

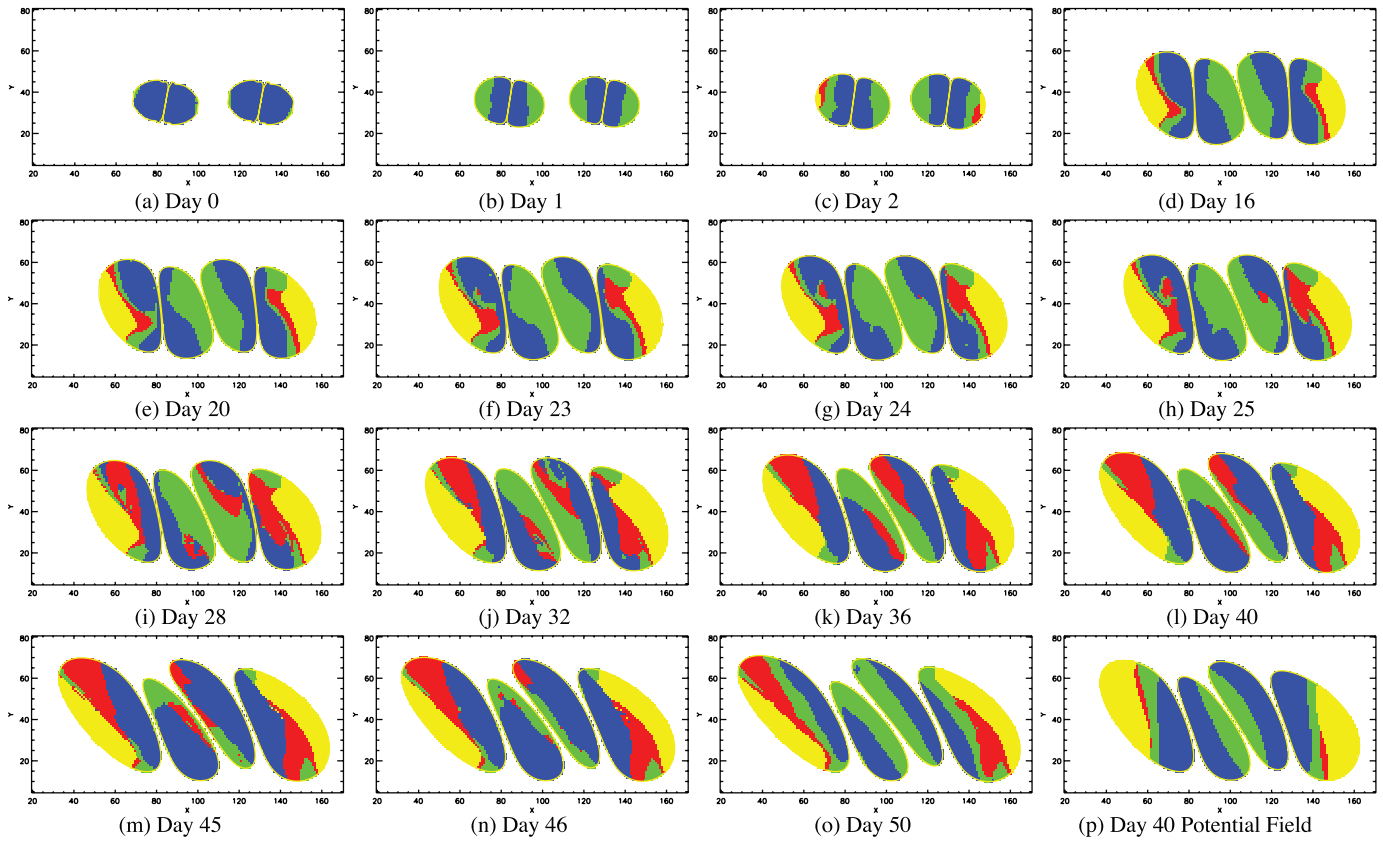

FIG. 1.—(*a*–*o*) Examples of the changing connectivity of the two bipoles as they interact. Blue represents bipolar connectivity, green represents cross-bipolar, red represents open flux, and yellow represents periodic flux. (*p*) Example of a connectivity map for a potential field deduced from the same radial field distribution on day 40.

lines are pushed out to the sides of the computational box, where they may pass through the periodic boundaries (Fig. 3*a*). On the left-hand side of the domain oppositely oriented open field lines may encounter one another and reconnect to produce periodic field lines and U-loops (o + o → p + U-loop). The U-loops are then expelled from the computational domain under the effect of the radial outflow velocity. From day 2 onward all four types of photospheric connectivity are present. The process described above (b + b → cb + cb, cb → o, and o + o → p + U-loop) slowly continues for the next day, by which time the average force within the box drops by over 2 orders of magnitude (Paper I, Fig. 5), and all closed field lines approach equilibrium. The transition from one connectivity type to another can be clearly seen in Figure 2*a*. From day 3 onward the connectivity domains have the same structure as that shown for day 2; the amount of flux within each domain remains roughly constant, and changes are mainly due to surface cancellation, suggesting that a stable connectivity situation has arisen. At this point the shearing phase of the simulation starts.

3.2. *Shearing Phase*

From day 3 onward the large-scale connectivity domains change very slowly from one day to the next. During this phase the initial shear in the coronal field is further enhanced by flux cancellation, and flux ropes form above the internal PIL of each bipole and the external PIL between the bipoles (see Paper I, § 3). In addition, the surface motions also cause an increase in the magnitude of the electric current across the quasi separator that lies in the corona between the two bipoles (Aulanier et al. 2005). As each of the bipoles is given a different initial twist, the shearing phase lasts a different length of time along each of the PILs. To describe a typical shearing phase, the field evolution above the trailing bipole is considered between days 3 and 18, beyond which the first ejection phase starts. Although the ejection phase for the trailing bipole starts on day 18, the shearing phase still continues along the other two PILs.

To consider the connectivity changes during the shearing phase, Figures 1*c* and 1*d* show the connectivity domains on days 2 and 16. It is clear from Figure 1*d* that over this 14 day period the same structure of the photospheric connectivity domains is found, with the only variation the physical extent of each domain. Therefore, over this period the coronal field maintains its same global structure. There is, however, a clear progression of the cross-bipolar flux (*green*) toward the internal PILs of each bipole. This progression indicates that flux with bipolar connectivity is slowly being removed from above the bipoles and converted into cross-bipolar flux (b + b → cb + cb). From Figure 2*a* this can be seen by the bipolar flux decaying faster than the total flux. Although cross-bipolar flux is produced, there is no net increase in it, but rather there is a net increase of open and periodic flux as they are subsequently produced from the cross-bipolar flux.

The changes in the coronal field structure associated with the connectivity domains can be seen in Figure 3, where field lines are shown on day 3 (Fig. 3*a*) and day 16 (Fig. 3*b*). The selected field lines lie close to a surface of constant latitude through the center of the bipoles. The surface diffusion and differential rotation cause the bipoles to expand. During this expansion bipolar field lines of opposite orientation are pushed together at the quasi separator between the two bipoles. As the trailing bipole is inserted with a higher degree of twist (β), it rises faster than the leading bipole, resulting in the quasi separator being pushed to the right (Fig. 3*b*). This expansion drives a reconnection process

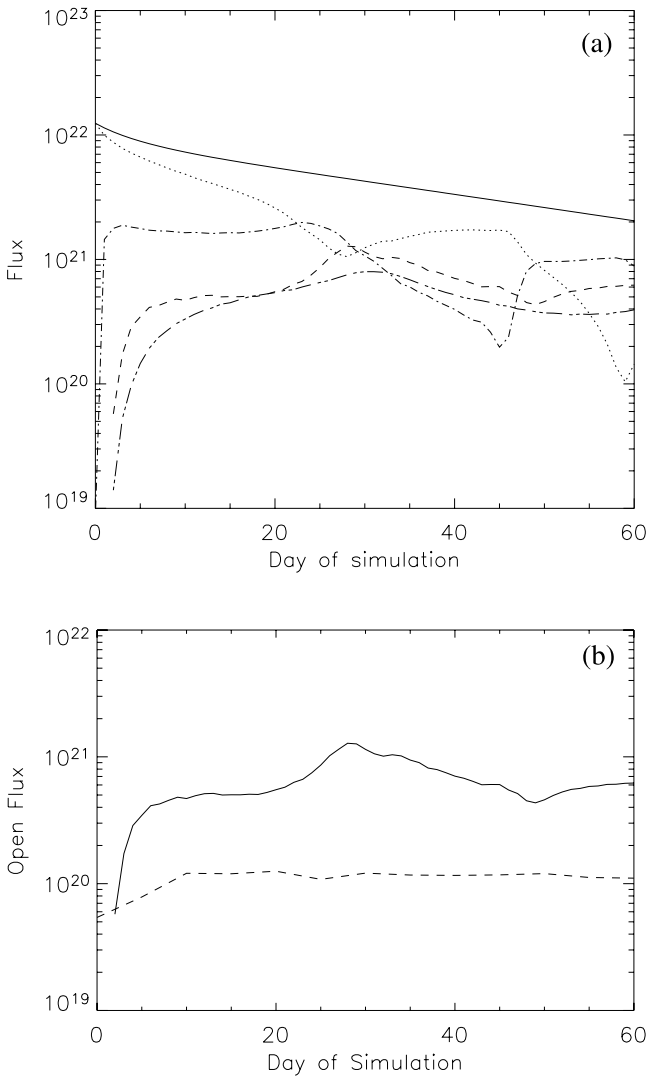

FIG. 2.—(*a*) Graph of the variation of the net unsigned flux in the various connectivity domains summed over all the bipole polarities as a function of the day of simulation. The dotted line denotes bipolar flux, the dash-dotted line denotes cross-bipolar flux, the dashed line denotes open flux, and the double-dot-dashed line denotes the periodic flux. The solid line denotes the sum of all the individual connectivity domains. (*b*) Graph of the variation of the open flux vs. day of simulation. The solid line represents the results for the nonpotential simulations, while the dashed lines gives the results for a potential field deduced from the same surface distributions.

at the quasi separator, where bipolar flux is converted into cross-bipolar flux. Initially it is the highest bipolar field lines (those with footpoints farther away from the internal PILs) that reconnect first. Once these have been reconnected, those lower down may rise and follow a similar process. Hence, there is a gradual conversion of bipolar to cross-bipolar flux in the shearing phase as seen in Figure 1, where the boundary between the two regions moves steadily toward the internal PIL. From Figure 1*d* it is also clear that the conversion of bipolar to cross-bipolar flux does not occur symmetrically, as the cross-bipolar flux lies much closer to the internal PIL of the more highly twisted trailing bipole than the less twisted leading bipole.

During the shearing phase the steady conversion of bipolar to cross-bipolar flux slowly strips away high bipolar arcades from above the internal PIL of each bipole and adds flux both low down and high above the external PIL between the bipoles. This gradual stripping away of the bipolar flux helps the initial rise of the flux ropes and their subsequent ejection. The evolution described above then continues until day 18, when a flux rope starts to lift off and field lines start to be reconnected below it (see § 5 of Paper I). At this point more significant changes may occur to the connectivity domains, which are discussed in § 3.3.

3.3. *Ejection Phase*

During the shearing phase the global connectivity domains of the bipoles evolve slowly. However, once the liftoff of a flux rope starts, coronal reconnection occurs underneath the rising flux rope (see Paper I, § 5), rapidly producing new connectivity domains. The formation of these domains and the subsequent ejection of the flux ropes is now considered. Emphasis is given to the reconnection process occurring at the quasi separatrix layer (QSL; Priest & Démoulin 1995) formed through the distortion of the coronal field underneath the flux rope above the trailing bipole, as it is the first one to lift off. The first set of reconnections that occur at this QSL are those that result in a significant amount of shear being maintained along the internal PIL of the trailing bipole (see Paper I, Fig. 7).

3.3.1. *Maintaining the Shear above the PIL*

The initial set of coronal reconnections that occur at the QSL, formed below the flux rope above the trailing bipole when the flux rope lifts off, are such that they do not significantly alter the photospheric connectivity domains. This can be seen in Figures 1*e* and 1*f*, which show the connectivity maps on day 20 and 23. Between days 18 and 21 the main reconnection that occurs underneath the flux rope is between high bipolar field lines. Examples of these reconnecting field lines can be seen in Figure 4 (*top left*), showing the field lines from above and the side on day 20. These two field lines reconnect in the corona between days 20 and 21 (Fig. 4, *bottom left*) to create a large loop with a significant dip, along with a much shorter low-lying loop over the PIL on day 21. Due to the fact that the footpoints of the reconnecting loops are displaced from one another, the low loop maintains a significant shear during the liftoff. The large-scale loop forms above the QSL and then is located underneath the flux rope. As it has a large radius of curvature, to attain equilibrium, it straightens out and in the process helps to push the flux rope out of the box. This reconnection process, which involves the exchange of bipolar footpoints ($b + b \rightarrow b + b$), does not alter the connectivity domains. However, while this process is occurring, bipolar field lines are still being reconnected into cross-bipolar at the quasi separator that is located high in the corona between the two bipoles, as described in the previous section. Therefore, the amount of bipolar flux still continues to decrease (Fig. 2*a*), as it is both canceled due to photospheric flux cancellation and converted into cross-bipolar flux. This continual decrease of the bipolar flux allows the cross-bipolar flux to continue to approach the internal PIL (compare the connectivity maps on day 16 and 20).

By day 21, a significant amount of the high bipolar flux has been reconnected at the QSL lying in the corona above the trailing bipole. From now on cross-bipolar field lines that are approaching the PIL may start to reconnect at the QSL formed below the flux rope. This can be seen in Figure 4 (*top right*), where a cross-bipolar field line (on day 21) connecting the two outer polarities reconnects with a bipolar field line ($cb + b \rightarrow cb + b$) by day 22 (*bottom right*). The resulting field lines can be seen on day 22 to produce a low, strongly sheared bipolar field line and a high coronal loop that is dipped. In contrast to the previous reconnection, which maintained exactly the same connectivity domains, these reconnections transport the footpoints of the cross-bipolar field lines away from the PIL into the center of each bipole. In

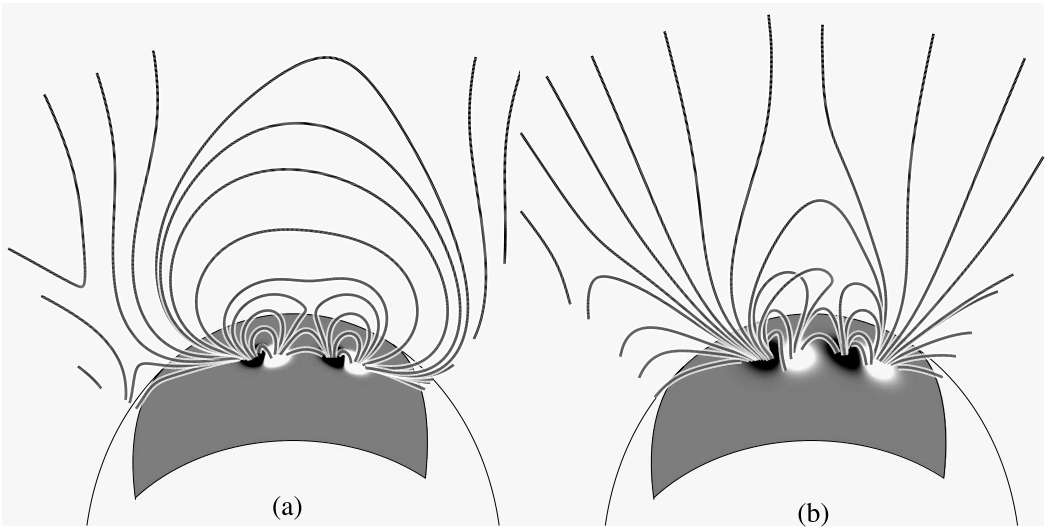

FIG. 3.—Examples of the coronal field structure on (*a*) day 3 and (*b*) day 16. In each image the gray-scale image represents the surface magnetic configuration, in which white represents positive flux, and black negative flux, where each is set to saturate at ±5 G. The field on day 16 is significantly more sheared than that on day 3.

Figure 1 this transport of the cross-bipolar field lines (*green*) into the center of the bipole can be seen by considering the connectivity maps on day 20 (Fig. 1*e*) and day 23 (Fig. 1*f*). A significant consequence of this reconnection is that once the cross-bipolar flux has been transported away, the open flux behind it may then approach the internal PIL of the trailing bipole and start to reconnect, resulting in the large-scale transport of the open flux, which is described next.

3.3.2. *Large-Scale Transport of Open Flux by Interchange Reconnection*

Before day 23 the reconnection that occurs below the flux rope above the trailing bipole at the QSL does not significantly alter the connectivity domains. However, from day 23 onward this is no longer true. From this point, new connectivity domains of open flux are produced, as previously open field lines reconnect with closed loops through "interchange reconnection" (Crooker et al. 2002) resulting in the large-scale transport of open flux across the bipoles. This can be seen for days 23–25 in Figure 5 for the reconnecting field lines and in Figures 1*f* through 1*h* for the photospheric connectivity domains.

On day 23 the transport of open flux across the negative polarity of the trailing bipole occurs as open flux approaches the internal PIL and is reconnected with bipolar flux ($o + b \rightarrow o + b$). The resulting changing connectivity of the field lines can be seen in the left-hand column of Figure 5, where the field lines are

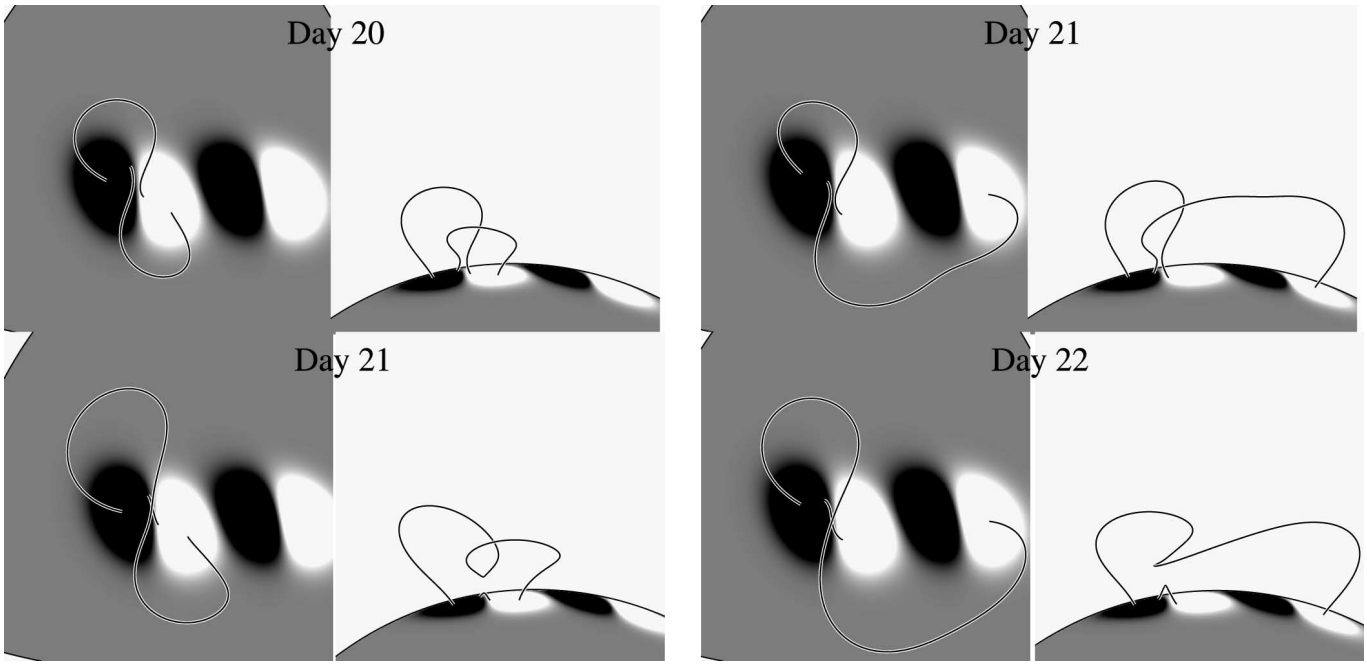

FIG. 4.—Typical examples of reconnecting field lines between days 18 and 22, when the reconnection occurs underneath the flux rope. Field lines are shown before and after reconnection in the top and bottom panels, respectively, for days 20–21 (*left*) and 21–22 (*right*). Each of the reconnections produces a high arcade, which helps to push the flux rope out, and a low, strongly sheared arcade, which maintains the shear along the PIL.

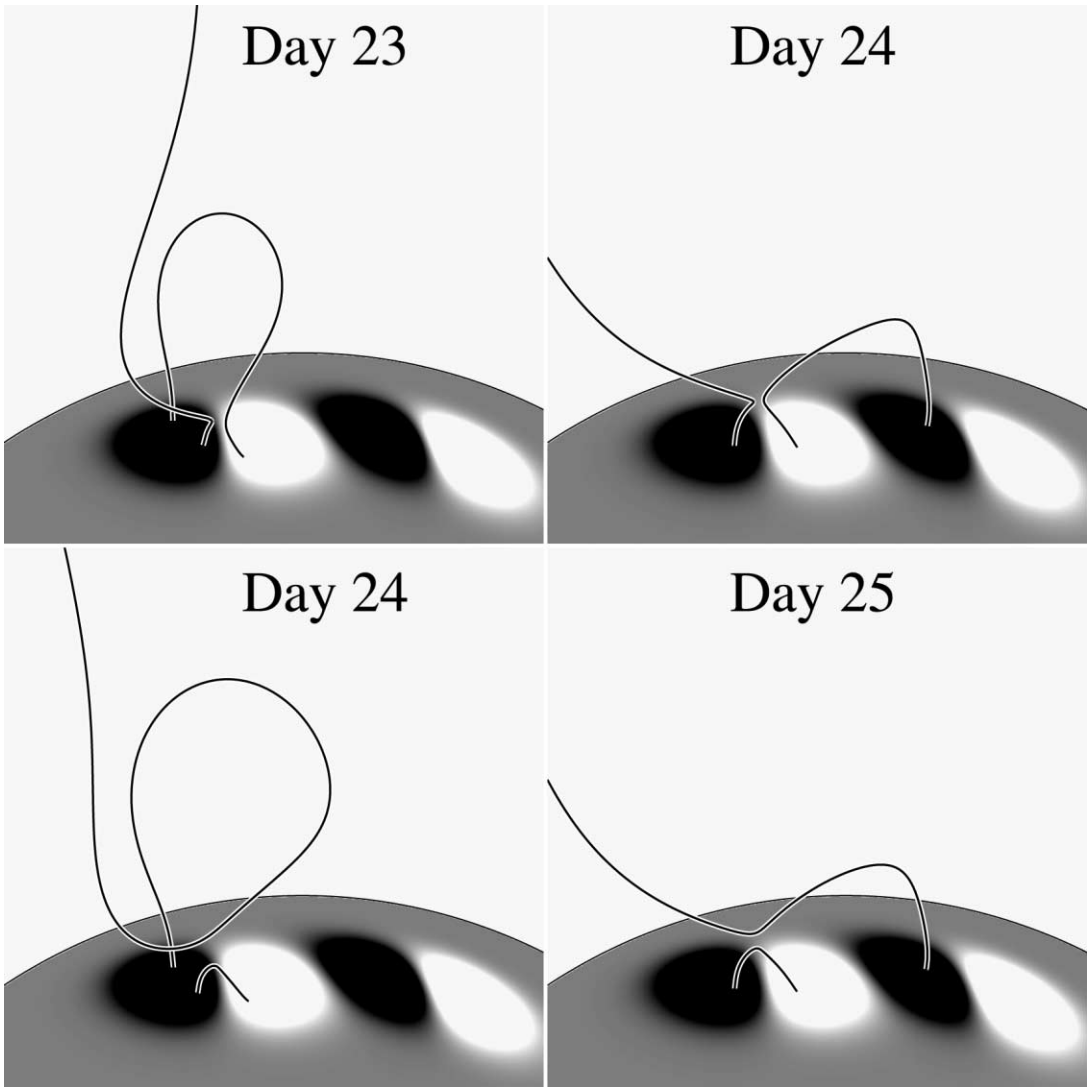

FIG. 5.—Typical examples of reconnecting field lines between days 23 and 26, when the reconnection occurs underneath the flux rope. Field lines are shown before and after reconnection in the top and bottom panels, respectively, for days 23–24 (*left*) and 24–25 (*right*). Each of the reconnections translates the open flux across the bipoles by "interchange reconnection."

shown before and after the reconnection on days 23 and 24, respectively. After reconnection the open field line can be clearly seen to have its footpoint displaced north. As before, the reconnection process produces a sheared arcade lying over the internal PIL at low heights. The effect of this process is that it strips away more of the high bipolar flux lying above the flux rope and makes it easier for the flux rope to escape. However, it does not alter the total flux lying within each of the domains. The resulting change in the connectivity domains can be seen by comparing Figures 1*f* and 1*g*, where between these two days an island of open flux (*red*) can clearly be seen to form at the northern end of the negative polarity of the trailing bipole. With this transport the coronal field becomes very complicated, with open and closed field lines interweaved between one another.

By day 24 the coronal reconnection process described above has stripped away a significant amount of the bipolar flux lying above the flux rope, and with this the flux rope is now free to leave the box. Once the vast majority of the high bipolar flux is stripped away, the large-scale transport of open flux then continues, as open flux from the negative polarity of the trailing bipole reconnects with cross-bipolar field lines that connect between the two bipoles low down over the external PIL ($o + cb \rightarrow o + b$). This can be seen in the right-hand column of Figure 5, where the reconnection has a twofold effect. First, new bipolar flux is created low over the internal PIL of the trailing bipole at the expense of cross-bipolar flux. Second, there is large-scale transport of open flux from the negative polarity of the trailing bipole to the negative polarity of the leading bipole. In doing so, a new connectivity domain is created, even though the net amount of open flux stays the same (compare Figs. 1*g* and 1*h*).

3.3.3. *Liftoff of Flux Rope above Leading Bipole and Opening of Closed Flux*

From day 26 onward the flux rope that forms and lies above the internal PIL of the leading bipole starts to lift off. With this another QSL now forms underneath it, where reconnection may occur. The evolution of the connectivity domains now becomes very complicated, as first field lines may reconnect at one QSL and then the other. While all these reconnections have been studied in detail, only the main sets of reconnections that alter the connectivity domains are described below.

On comparing the connectivity maps of the leading and trailing bipoles before the liftoff occurs on each of them (Figs. 1*h* and 1*d*), it is clear that the two connectivity maps are very different. The

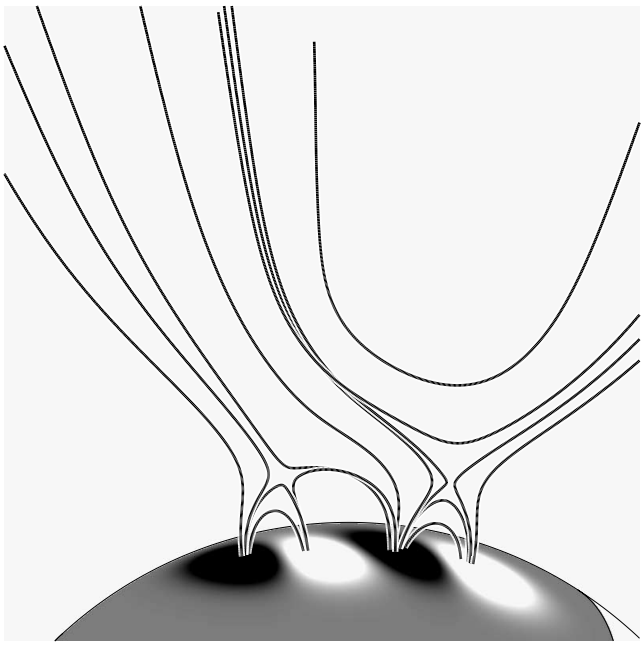

FIG. 6.—Coronal field configuration from day 27 once the flux rope lifts off from the leading bipole. Field lines undergo a two-stage reconnection process to produce U-loops, with the reconnection first occurring above the trailing bipole, then the leading bipole.

main difference is that for the leading bipole, where the liftoff occurs later, the open flux occupies a much larger area and lies much closer to the internal PIL when the liftoff starts. Thus, the open flux plays an important role in the evolution of the flux rope above the leading bipole as it is expelled. In fact, by looking back over the photospheric connectivity maps from day 20 onward and Figure 2*a*, it is clear that the open flux within the simulation is steadily increasing during this period. The reason why it is increasing and lies so close to the internal PIL on the leading bipole is that as the flux rope from the trailing bipole rises, it pushes open the cross-bipolar flux lying above it (cb $\rightarrow$ o), decreasing the cross-bipolar flux, but increasing the amount of open flux (see Fig. 2*a*). This also produces the new region of open flux at the southern end of the positive polarity of the trailing bipole between days 25 and day 28 (Figs. 1*h* and 1*i*).

3.3.4. *Formation of U-Loops*

From day 27 onward, once the QSL has formed above the internal PIL of the leading bipole, all subsequent coronal reconnection of the field lines and changes in their connectivity domains occur in a twofold process between both bipoles. The exact order in which the reconnection occurs depends on whether it takes place north or south of the bipole centers. In Figure 6, the results can be seen for field lines lying north of the center of the bipoles.

The first stage in the creation of the U-loops starts above the trailing bipole, where open field lines reconnect with cross-bipolar field lines to transport footpoints of the open field lines across the bipoles and produce a bipolar field line (o + cb $\rightarrow$ o + b) over the trailing bipole. Once formed, these open field lines slide to the right under the action of the tension force. As they do so, they may then reconnect at the QSL above the lead PIL with another open field line to produce a bipolar one and a U-loop (o + o $\rightarrow$ b + U-loop). Subsequent reconnection then pushes the U-loops up, and the radial outflow causes the U-loops to be expelled from the box. The reconnection above the leading bipole occurs between open field lines with strongly displaced footpoints, and this reconnection maintains the shear above the internal PIL of the leading bipole. For locations equatorward of the center of the bipoles the same process occurs, but first above the leading bipole (o + cb $\rightarrow$ o + b) and then above the trailing bipole (o + o $\rightarrow$ U-loop + b). The net effect is an enhancement in the amount of bipolar flux in the simulation at the expense of cross-bipolar and open flux. This can been seen in Figure 2*a*, where from day 27 onward the bipolar flux steadily increases, while the open and cross-bipolar flux decreases. The reconnection also begins to strip away the cross-bipolar flux that was produced low down over the external PIL earlier on in the simulation. Correspondingly the changes in the surface connectivity maps can be seen in Figures 1*i* through 1*l* for days 28–40, over which the same coronal reconnection process continues. Through this the coronal field relaxes back to equilibrium (see Paper I, Fig. 5) and all signs of the first two flux ropes disappear. The ejection of the second flux rope occurs much faster than the first, as during the first a significant amount of bipolar flux from both bipoles is converted into cross-bipolar

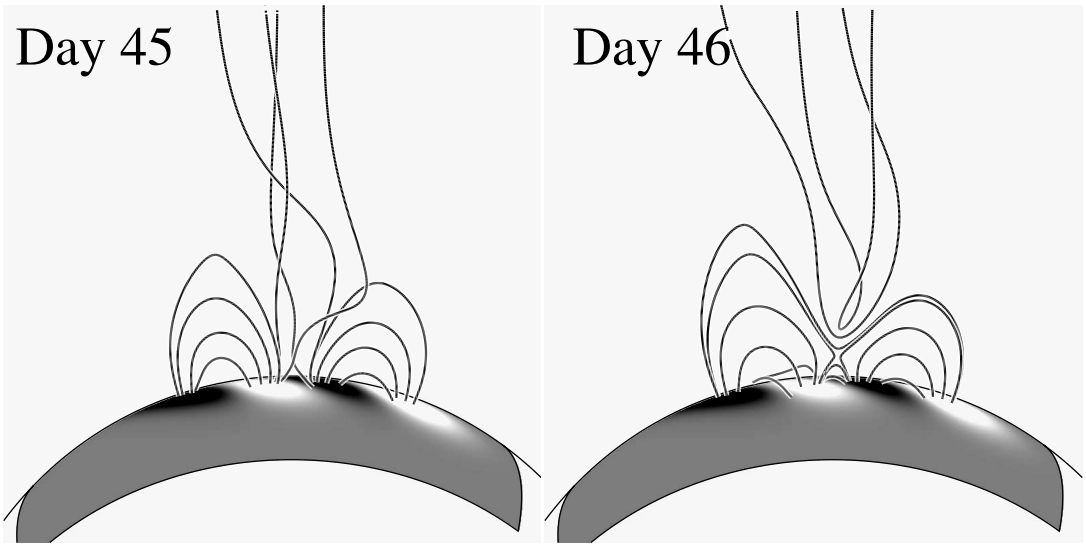

FIG. 7.—Coronal field configuration on day 45 (*left*) and day 46 (*right*), showing the field before and after the liftoff above the external PIL. Open field lines reconnect to produce U-loops that lie underneath the flux rope being ejected.

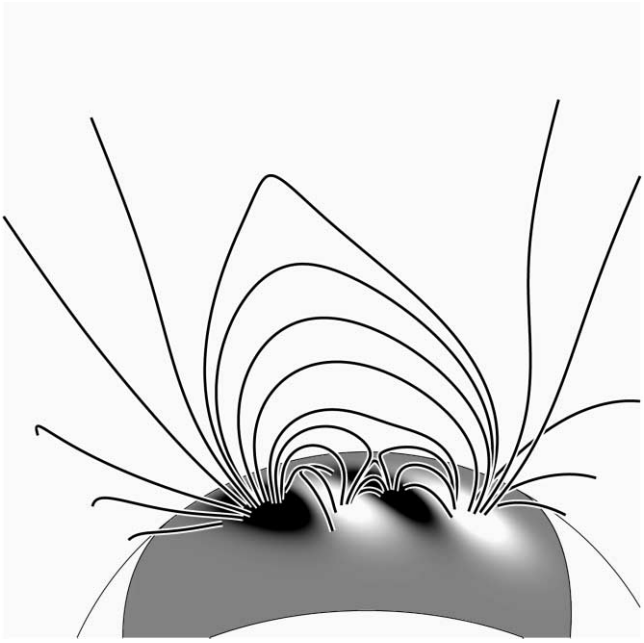

FIG. 8.—Coronal field configuration on day 50 once all three flux ropes have been ejected. The field relaxes to a configuration similar to that of the shearing phase.

flux, then open flux, making it much easier for the second flux rope to rise.

3.4. *Liftoff at External PIL and Field Closedown*

By day 40 the third flux rope above the external PIL has fully formed, and on day 45 it starts to lift off, with another QSL forming below it through the distortion of the coronal field. The reconnection that occurs at this QSL is much simpler than before. The field structure is shown in Figure 7, and the connectivity maps for days 45 and 46 are given in Figures 1*m* and 1*n*. This time the reconnection only involves open field lines that lie on either side of the external PIL (see Fig. 7, *left*). As shown in Figure 7 (*right*), the field lines reconnect with each other over a period of a single day to produce cross-bipolar flux and U-loops that are subsequently pushed out of the box (o + o $\rightarrow$ cb + U-loop).

This set of reconnections proceeds extremely fast, and by day 46 most of the open flux has reconnected. This can be seen by comparing Figures 1*m* and 1*n*, where between these two days the open flux (*red*) disappears from either side of the external PIL. Once this is complete, bipolar field lines from each of the bipoles then start to reconnect at a new quasi separator above the external PIL to produce cross-bipolar flux (b + b $\rightarrow$ cb + cb). The coronal field then returns to a configuration similar to that described within the shearing phase of the simulation on days 4–18, where the amount of bipolar flux steadily decreases with the production of cross-bipolar flux (see Fig. 2*a*). Finally, in Figures 1*o* and 8 the resulting surface connectivity map and coronal field lines can be seen on day 50. It is clear that the magnetic configuration has returned to a state very similar to that found during the shearing phase. This simulation has been continued for a further 40 days under the same surface effects, where it is found that exactly the same evolution of the coronal field as described above occurs again, where first flux ropes form above each PIL and subsequently lift off. The only difference between the first and second series of formations and liftoffs is that the formation time is less, as significant shear is left on each of the PILs after the first ejections occur.

4. VARIATION OF OPEN FLUX

In recent years there has been much interest in studying through observations (Lockwood et al. 1999; Wang et al. 2000a) and theory (Fisk & Schwadron 2001; Mackay et al. 2002; Mackay & Lockwood 2002; Fisk 2005) the variation of the Sun's open magnetic flux. The reason is that variations in the open flux have been linked to variations in the Earth's climate (Svensmark & Friis-Christensen 1997; Svensmark 1998; Bond et al. 2001; Lockwood 2001, 2002), as well as to many effects in the near-Earth environment studied as part of space weather. Lockwood et al. (1999) and Wang et al. (2000a) showed through different techniques that the open flux varies through the solar cycle by roughly a factor of 2 and that in each cycle the modulation of the open flux lags behind the total surface flux by roughly 1–2 yr (see also Wang & Sheeley 2002). To predict how the interplanetary magnetic field (IMF) may affect us in the future, we need to understand both the origin of the Sun's open flux and its variations as magnetic fields are diffused and advected across the solar surface.

The Sun's open flux may have two contributions: a slowly varying component produced by solar active regions as they emerge and decay and a more rapidly varying component associated with coronal mass ejections (CME). The CME contribution is probably at most of order 20% at sunspot maximum (Wang & Sheeley 2002). Currently, it is unclear exactly how the "open" fields close to the Sun are connected to the open field measured at 1 AU. The lack of observed heat flux dropouts of superthermal electrons in the heliosphere suggests that U-loop structures in the solar wind are very rare (McComas et al. 1989, 1992). Therefore, we assume that CME-related increases in open flux near the Sun will eventually show up in the open flux at 1 AU (perhaps with some time delay).

Wang & Sheeley (1995, 2002) and Wang et al. (2000a) studied the variation of the Sun's open flux during the period 1971–1998. Using magnetograph data from Wilcox Solar Observatory (WSO) and Mount Wilson Observatory (MWO), they constructed potential field source surface (PFSS) models in which the corona is assumed to be current-free ($\boldsymbol{j} = 0$). The WSO and MWO data were recalibrated to account for magnetograph saturation effects, which significantly affect the latitude dependence of the surface fields and therefore the predicted open flux variations. The source surface radius was assumed to be constant in time, $R_{\rm ss} = 2.5\,R_{\odot}$. The Sun's open magnetic flux, $\Phi_{\rm open}(t)$, as a function of time through the cycle, can be predicted from the PFSS models. *Ulysses* measurements have shown that at heliocentric distances of order 1 AU the magnitude $|B_r|$ of the radial component of the IMF is independent of latitude and longitude (e.g., Balogh et al. 1995); hence the predicted open flux can be converted into an estimate for $|B_r|$. Wang et al. compared the predicted $|B_r|$ with in situ measurements at 1 AU and found excellent agreement in both the magnitude of $|B_r|$ and its variations over the solar cycle (see Fig. 2 in Wang et al. 2000a). This shows that the PFSS model with constant $R_{\rm ss}$ is an excellent tool for predicting the long-term variations in the Sun's open flux, at least for the period 1971–1998. Note that, since the modeling is done directly from calibrated magnetic maps, the fit between observed and predicted IMF does not depend in any way on assumptions about surface flux transport or the sizes, tilts, and emergence rates of solar active regions through the solar cycle.

Another method for modeling the Sun's open flux is to combine the PFSS model with simulations of the emergence and transport of magnetic flux at the solar surface (e.g., Wang et al. 1996, 2000b; Schrijver & DeRosa 2003). Mackay & Lockwood (2002)

carried out full solar cycle simulations that tried to reproduce the observed phase lag between the surface activity and the open flux. It was found that the observed phase lag of 1–2 yr could not be reproduced with any realistic combination of the parameters describing the surface flux transport and PFSS models. Mackay & Lockwood (2002) concluded that PFSS models probably do not contain the correct physics to describe the origin of the phase lag in the open flux over the solar cycle and that nonpotential field models should be considered. A different full-cycle transport model (for Cycle 21) was developed by Wang et al. (2002). To account for the change in the calibration of the WSO and MWO data, they increased the strengths of the bipole sources by a factor of 3 compared to their earlier model (Wang et al. 1989). Wang et al. (2002) found that by increasing the meridional flow velocity at low latitude and reducing the diffusion constant, they could obtain good agreement between the observed and predicted values of the global dipole, which is the main determinant of the open flux in the PFSS model. They also found good agreement between the observed and predicted radial IMF at 1 AU (see Fig. 7*b* of their paper). The model even reproduces the peak in the IMF radial field observed in 1982; this peak is largely responsible for the observed time lag in Cycle 21. More recently, Wang et al. (2005) have extended their model over 26 solar cycles.

Although the PFSS model successfully predicts the long-term variations of the open flux, the model probably does not provide an accurate description of the short-term variations (timescale of days) and the spatial distribution of the open flux in the corona. This is especially true around cycle maximum, when strong electric currents are known to exist in the corona. In the simulations presented here, where simple two-bipole interactions are considered and the coronal field is nonpotential, a significant variation of the open flux in both strength and location is found. These variations are described in more detail below. While we are only considering a limited region, the amount and variation of the open flux seen here could represent a low-latitude contribution to the open flux of the Sun during periods of high activity.

In Figure 2*b* it is clear that the open flux (*solid line*) varies significantly from its initial value over the period of the simulation. First, there is an increase in open flux during the first few days of the simulation, as the bipoles expand into the coronal volume and the magnetic field adjusts to the radial outflow velocity imposed near the upper boundary. The open flux increases from about 6×10^{19} to 4.5×10^{20} Mx. Next, during the shearing phase (days 3–18), the bipoles are in a nonpotential equilibrium and the open flux remains relatively constant at a value of about 4.5×10^{20} Mx. Finally, there is a temporary increase in open flux during the liftoff, as closed field lines are opened and reconnected.

The dashed curve in Figure 2*b* shows the open flux derived from a PFSS model with source surface located at the upper boundary of our computational domain ($R_{ss} = 2.5\ R_{\odot}$). It is clear that the PFSS model has a much lower value of open flux ($\sim 10^{20}$ Mx) that does not vary significantly over the 60 day period of the simulation. The increased value of open flux in the nonpotential model is mainly the result of the radial outflow imposed near the upper boundary of the domain. This outflow causes the opening of high-altitude field lines that are closed in the PFSS model. Therefore, the "effective source surface radius" R_{ss} for the nonpotential model lies somewhat below the outer boundary of the computational domain. In future numerical studies the outer radius will be increased, so that the effective R_{ss} matches the value used in PFSS modeling of the long-term variations of the Sun's open flux (Mackay & Lockwood 2002; Wang & Sheeley 2002; Wang et al. 2000a, 2005).

In Figure 1*p* the surface connectivity map can be seen for a PFSS model on day 40. It is clear that this map bears no resemblance to the connectivity map for the nonpotential field, implying that the open fields are significantly affected by coronal electric currents. Potential field maps have been constructed for each day in the simulation, and results similar to those shown in Figure 1*p* are always found. Note that the value of the open flux on day 50 is approximately equal to its "equilibrium" value of about 4.5×10^{20} Mx, but the connectivity maps for the potential and nonpotential fields on that day are quite different. Therefore, the fact that the open flux of the Sun is close to its equilibrium value cannot be taken as evidence that the open field has a simple structure similar to that of a potential field.

During the liftoff and ejection of the flux ropes the amount of open flux temporarily increases from its base level of 4.5×10^{20} Mx on days 5–20 to 1.3×10^{21} Mx on day 29 before returning to its (nonpotential) equilibrium value. Therefore, during the simulation the open flux varies by just over a factor of 2. This shows that during such ejections the amount of open flux within each bipole increases significantly. To properly simulate an eruption and associated open flux enhancement, a full MHD model would be required. However, the same amount of overlying closed flux would have to be opened in the process. Therefore, the magnitude of the open flux enhancement in a full MHD simulation would likely be similar to that found here.

Care must be taken in comparing the duration of open flux enhancement to that for eruptions on the Sun. Since we use a magnetofrictional approach, we do not follow the true dynamics of the coronal field and plasma as it erupts, and the duration of the open flux enhancement is longer than that expected for the Sun. The true duration of open flux enhancements associated with CMEs on the Sun is not known, but observations of coronal dimmings (Hudson & Webb 1997) suggest a period of 1–2 days, somewhat longer than the dynamical timescale of the eruptions. Assuming that on average each active region erupts once every 20 days (as suggested by the duration of the shearing phase in our simulation) and that the open flux is enhanced by factor of 2 for a period of 2 days, the estimated contribution of CMEs to the Sun's open flux at cycle maximum is about 10%. Therefore, the contribution from CMEs to the Sun's open flux is relatively small and cannot account for the factor of 2 variation seen in the course of the activity cycle. This larger variation must be due to more gradual changes in the "equilibrium" open fluxes of the active regions as new regions are born and old regions decay.

Another interesting feature of the simulations is that the locations of open field lines are transported over large distances across the bipoles through a process of "interchange reconnection" with closed loops (Crooker et al. 2002; Fisk & Schwadron 2001; Fisk 2005). As a result, new locations of open field are created in the central portions of the bipoles. Although new regions of open flux are produced, this interchange reconnection does not alter the net amount of open flux. Such a feature has been discussed in the models of Fisk & Schwadron (2001) and Fisk (2005). The large-scale transport of open flux not only helps to open up the field lines above the ejecting flux rope, but also increases the complexity of the coronal field; open and closed field lines lie intertwined among one another.

5. CONCLUSIONS

In the paper of Mackay & van Ballegooijen (2006, Paper I) the evolution of the large-scale coronal magnetic field was considered through magnetic flux transport and magnetofrictional relaxation simulations. The simulations considered the formation of nonlinear force-free fields due to large-scale surface motions

and surface diffusion on the Sun. It was shown that, as two bipolar magnetic regions interact, magnetic flux ropes may form through photospheric reconnection driven by flux cancellation. Once the flux ropes form along either the internal PIL within the bipoles or external PIL between the bipoles, the coronal field may diverge from equilibrium with the ejection of the flux ropes.

In the present paper the changing connectivity of the coronal field due to coronal reconnection occurring during the formation and ejection of the flux ropes was described. Such reconnection is required to open up coronal arcades lying above the flux ropes to enable the flux ropes to leave the computational box. To describe the changing connectivity of the coronal field, four distinct types of photospheric connectivity domains are considered. These include bipolar connectivity, where field lines connect between the polarities that make up the original bipoles; cross-bipolar connectivity, where field lines connect between the two bipoles; open connectivity, where field lines extend out to the source surface at 2.5 $R_\odot$; and periodic connectivity, where field lines pass through the periodic ϕ-boundaries. For the 60 day simulation period considered it is found that photospheric reconnection (which forms the flux ropes) does not alter the field line connectivity domains within each bipole. This, however, is not true for coronal reconnection, which may convert flux from one domain to another.

Throughout the simulation coronal reconnection may occur both before and after the flux ropes form. Those occurring before take place high in the corona along a quasi separator that forms between the two bipoles. At this location sheared coronal arcades rise up and slowly reconnect to reconfigure the coronal field over a large number of days. By doing so arcades overlying the flux ropes are slowly stripped away, allowing the flux ropes to escape. Once the flux ropes rise, this process speeds up. Coronal reconnection may also occur below the flux ropes at multiple QSLs, which form as the flux ropes lift off. At these QSLs a wide variety of field lines from the various connectivity domains may reconnect. This reconnection may either preserve the original connectivity domains or create new domains. It is found that the coronal reconnection that occurs underneath the flux ropes maintain a significant skew to the coronal arcades overlying the PIL. During the later stages reconnection underneath the flux ropes may result in both the small-scale transport of open flux within a single polarity of a bipole or the large-scale transport from one bipole to another. Such a process of "interchange reconnection" has been considered as the method through which open flux may be transported across the Sun (Fisk & Schwadron 2001; Fisk 2005). In the simulations interchange reconnection produces new open flux domains within the centers of each of the bipoles, where none previously existed. This shows that the structure of the open flux in a nonpotential field configuration may be very different from that of a potential field configuration.

A significant variation of the open flux is found throughout the simulations, where the amount of open flux may be split into two distinct contributions. The first is that due to the nonpotential field of the bipoles when they are in equilibrium. The second is an enhancement to this basic value during ejections, when closed field lines are forced open. It is found that the basic nonpotential equilibrium open flux is significantly higher compared to that of a potential field determined from the same photospheric boundary conditions. Also during the ejections the amount of open flux within the bipoles may increase by over a factor of 2. This indicates that the nonpotential nature of coronal fields during periods of high activity may significantly affect the amount of open flux on the Sun.

In this paper the changing connectivity of a simulated coronal field has been considered during the formation and ejection process of flux ropes as two magnetic bipoles interact. This shows a complex behavior in which a wide variety of changes in the coronal field structure is found. In future full-Sun simulations, such changes will be considered for many bipoles as they are advected across the Sun for periods of months to years to consider the formation of solar filaments and the variation of the Sun's open magnetic flux.

D. H. M. would like to thank the UK Particle Physics and Astronomy Research Council for financial support. The simulations were carried out on a SHRIF/PPARC-funded supercomputer located in St. Andrews.

REFERENCES

Amari, T., Luciani, J. F., Aly, J. J., Mikic, Z., & Linker, J. 2003, ApJ, 595, 1231
Amari, T., Luciani, J. F., Mikic, Z., & Linker, J. 1999, ApJ, 518, L57
Aulanier, G., & Démoulin, P. 1998, A&A, 329, 1125
Aulanier, G., Pariat, E., & Démoulin, P. 2005, A&A, 444, 961
Balogh, A., Smith, E. J., Tsurutani, B. T., Southwood, D. J., Forsyth, R. J., & Horbury, T. S. 1995, Science, 268, 1007
Bleybel, A., Amari, T., van Driel-Gesztelyi, L., & Leka, K. D. 2002, A&A, 395, 685
Bond, G., et al. 2001, Science, 294, 2130
Canfield, R. C., Hudson, H. S., & McKenzie, D. E. 1999, Geophys. Res. Lett., 26, 627
Crooker, N. U., Gosling, J. T., & Kahler, S. W. 2002, J. Geophys. Res., 107, 3
Fisk, L. A. 2005, ApJ, 626, 563
Fisk, L. A., & Schwadron, N. A. 2001, ApJ, 560, 425
Hudson, H. S., & Webb, D. F. 1997, in Coronal Mass Ejections, ed. N. Crooker et al. (Geophys. Monogr. 99; Washington: AGU), 27
Hundhausen, A. J. 1993, J. Geophys. Res., 98, 13177
Isenberg, P. A., Forbes, T. G., & Démoulin, P. 1993, ApJ, 417, 368
Leighton, R. B. 1964, ApJ, 140,1547
Lin, J., & Forbes, T. G. 2000, J. Geophys. Res., 105, 2375
Litvinenko, Y. E., & Wheatland, M. S. 2005, 630, 587
Lockwood, M. 2001, J. Geophys. Res., 106, 16021
———. 2002, A&A, 382, 678
———. 2003, J. Geophys. Res., 108, 7
Lockwood, M., Stamper, R., & Wild, M. N. 1999, Nature, 399, 437
Low, B. C. 2001, J. Geophys. Res., 106, 25141
Mackay, D. H., & Gaizauskas, V. 2003, Sol. Phys., 216, 121
Mackay, D. H., Gaizauskas, V., & van Ballegooijen, A. A. 2000, ApJ, 544, 1122
Mackay, D. H., & Lockwood, M. 2002, Sol. Phys., 209, 287
Mackay, D. H., Longbottom, A. W., & Priest, E. R. 1999, Sol. Phys., 185, 87
Mackay, D. H., Priest, E. R., & Lockwood, M. 2002, Sol. Phys., 207, 291
Mackay, D. H., & van Ballegooijen, A. A. 2001, ApJ, 560, 445
———. 2005, ApJ, 621, L77
———. 2006, ApJ, 641, 577 (Paper I)
Martens, P. C., & Zwaan, C. 2001, ApJ, 558, 872
Martin, S. F. 1998, Sol. Phys., 182, 107
McClymont, A. N., & Jiao, L., & Mikic, Z. 1997, Sol. Phys., 174, 191
McComas, D. J., Gosling, J. T., & Phillips, J. L. 1992, J. Geophys. Res., 97, 171
McComas, D. J., Gosling, J. T., Phillips, J. L., Bame, S. J., Luhmann, J. G., & Smith, E. J. 1989, J. Geophys. Res., 690, 7
Mikic, Z., & McClymont, A. N. 1994, in ASP Conf. Ser. 68, Solar Active Region Evolution: Comparing Models with Observations (San Francisco: ASP), 225
Nakagawa, Y., & Raadu, M. A. 1972, Sol. Phys., 25, 127
Pevtsov, A. A. 2002, Sol. Phys., 207, 111
Priest, E. R. 1982, Solar Magneto-Hydrodynamics (Dordrecht: Reidel)
———. 1989, Dynamics and Structure of Quiescent Solar Prominences (Dordrecht: Kluwer)
Priest, E. R., & Démoulin, P. 1995, J. Geophys. Res., 100, 23443
Régnier, S., Amari, T., & Kersalé, E. 2002, A&A, 392, 1119
Russell, C. T., Priest, E. R., & Lee, L.-C. 1990, Physics of Magnetic Flux Ropes (Geophys. Monogr. 58; Washington: AGU)

Rust, D. M., & Kumar, A. 1995, Sol. Phys., 155, 69
Schrijver, C. J., & DeRosa, M. L. 2003, Sol. Phys., 212, 165
Somov, B. V. 1992, Physical Processes in Solar Flares (Dordrecht: Kluwer)
Svensmark, H. 1998, Phys. Rev. Lett., 81, 5027
Svensmark, H., & Friis-Christensen, E. 1997, J. Atmos. Sol. Terr. Phys., 59, 1225
Török, T., & Kliem, B. 2005, ApJ, 630, L97
van Ballegooijen, A. A., Cartledge, N. P., & Priest, E. R. 1998, ApJ, 501, 866
van Ballegooijen, A. A., & Martens, P. C. H. 1989, ApJ, 343, 971
van Ballegooijen, A. A., Priest, E. R., & Mackay, D. H. 2000, ApJ, 539, 983
Wang, Y.-M., Hawley, S. H., & Sheeley, N. R., Jr. 1996, Science, 271, 464
Wang, Y.-M., Lean, J., & Sheeley, N. R., Jr. 2000a, Geophys. Res. Lett., 27, 505
———. 2005, ApJ, 625, 522
Wang, Y.-M., Nash, A. G., & Sheeley, N. R., Jr. 1989, ApJ, 347, 529
Wang, Y.-M., & Sheeley, N. R., Jr. 1995, ApJ, 447, L143
———. 2002, J. Geophys. Res., 107(A10), 1302
Wang, Y.-M., Sheeley, N. R., Jr., & Lean, J. 2000b, Geophys. Res. Lett., 27, 621
———. 2002, ApJ, 580, 1188
Welsch, B. T., DeVore, C. R., & Antiochos, S. K. 2005, ApJ, 634, 1395
Yang, W. H., Sturrock, P. A., & Antiochos, S. K. 1986, ApJ, 309, 383